Indonesian Journal of Electrical Engineering and Computer Science
Vol. 44, No. 1, October 2026, pp. 97~107
ISSN: 2502-4752, DOI: 10.11591/ijeecs.v44.i1.pp97-107

Deep learning for OCT-based retinal fluid segmentation in neovascular AMD: a systematic review

Driss Rifai, Ahmed Zellou
Software Project Management (SPM) Research Team, ENSIAS, Mohammed V University, Rabat, Morocco

Article Info

Article history:

Received May 10, 2026
Revised Jul 15, 2026
Accepted Sep 10, 2026

Keywords:

Deep learning
Neovascular AMD
Optical coherence tomography
Retinal fluid segmentation
Systematic review

ABSTRACT

Neovascular age-related macular degeneration (nAMD) is a leading cause of irreversible central vision loss, and optical coherence tomography (OCT) is the reference modality for monitoring its fluid biomarkers: intraretinal fluid (IRF), subretinal fluid (SRF), and pigment epithelial detachment (PED). Deep learning enables automated, reproducible fluid segmentation and volumetric quantification. This systematic review synthesizes 55 studies (2021–2025) on deep-learning fluid segmentation in nAMD OCT, structured around four research questions covering architectural evolution, dataset and domain generalization, compartment-level performance, and clinical translation. The evidence shows a clear progression from convolutional networks (dice up to 0.955 for SRF) toward attention-based, graph-based, and hybrid CNN–Transformer architectures, with self-supervised foundation models emerging as a route to label efficiency. IRF is consistently the most difficult compartment (dice ≈ 0.76–0.80), while subretinal hyperreflective material (SHRM) is an increasingly recognized fourth biomarker that current pipelines rarely target. Cross-vendor domain shift and the limited clinical interpretability of dice remain the principal unresolved challenges; volumetric reliability, rather than peak overlap accuracy, emerges as the key determinant of clinical adoptability.

This is an open access article under the CC BY-SA license.

Corresponding Author:

Driss Rifai
Software Project Management (SPM) Research Team, ENSIAS, Mohammed V University
Rabat, Morocco.
Email: driss_rifai@um5.ac.ma

1. INTRODUCTION

Neovascular age-related macular degeneration (nAMD) is a chronic, progressive retinal disease and a principal cause of irreversible central vision loss in older adults. It affects an estimated 196 million people worldwide, with projections approaching 288 million by 2040 [1]. Its pathological hallmark is choroidal neovascularization, which drives exudative fluid leakage, structural deformation, and photoreceptor degeneration. Sustained monitoring of disease activity is therefore essential to preserve vision and individualize therapy [2].

Optical coherence tomography (OCT) is the reference standard for diagnosing and monitoring nAMD. It resolves the principal biomarkers of exudative activity intraretinal fluid (IRF), subretinal fluid (SRF), and pigment epithelial detachment (PED) which guide anti-vascular endothelial growth factor (anti-VEGF) dosing decisions [2]. Figure 1 illustrates these compartments, together with subretinal hyperreflective material (SHRM), on representative OCT B-scans. In routine practice, OCT interpretation remains largely manual: it is labor-intensive, subject to inter-observer variability, and poorly suited to detecting subtle longitudinal change [3]. Deep learning addresses these limitations through objective, reproducible segmentation and volumetric quantification [4]. Convolutional neural networks (CNNs) already achieve Dice

coefficients exceeding 0.90 for well-defined compartments such as SRF and PED [5], [6], while attention-based, graph-based, and Transformer-based architectures have improved robustness and cross-domain generalization [7]–[12].

Three challenges persist. First, IRF segmentation lags behind SRF and PED because of small lesion size, low tissue contrast, and fragmented morphology [6], [7]. Second, cross-vendor domain shift degrades performance when models are transferred across OCT platforms [13]. Third, the Dice coefficient inadequately reflects clinical relevance, since volumetric reliability—not pixel overlap—governs longitudinal monitoring [3]. A fourth biomarker, SHRM, is increasingly documented as prognostically important yet rarely targeted by automated pipelines [14], [15].

Existing reviews address deep learning broadly across ophthalmology [16] or summarize retinal fluid segmentation architectures without a structured, nAMD-specific protocol [17]. This review fills that gap. It provides a protocol-driven systematic synthesis of deep-learning fluid segmentation specifically for nAMD OCT (2021–2025), organized around four research questions as shown in Tables 1 and 2.

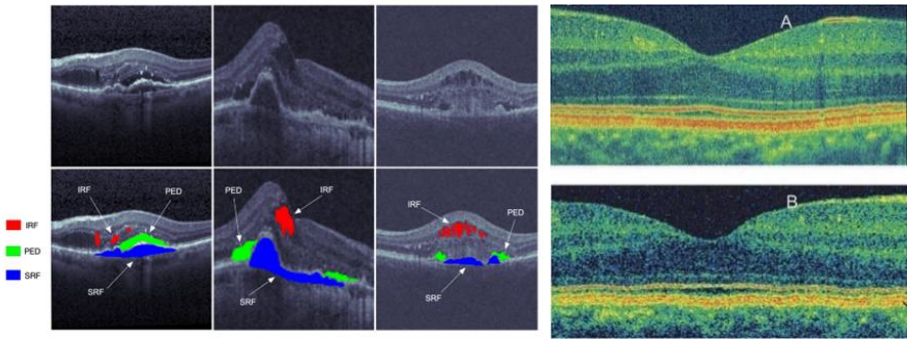

Figure 1. Representative OCT B-scans illustrating the principal retinal fluid compartments in nAMD: IRF, SRF, PED, and SHRM

Table 1. Research questions

RQ	Focus	Question
RQ1	Architecture	How have segmentation architectures evolved, and which design components most influence performance?
RQ2	Data / generalization	How do dataset characteristics, annotation, and domain adaptation affect cross-vendor robustness?
RQ3	Performance	How does accuracy compare across IRF, SRF, PED, and SHRM, and which compartment is most challenging?
RQ4	Clinical translation	How has automated fluid quantification influenced clinical decision-making and treatment monitoring?

Table 2. Quality-assessment summary by class. Full per-study data available on request

Class	n	%	Studies (S-IDs)
High (≥4.5)	28	50.9%	S01, S04, S07, S08, S10, S11, S13, S15, S17, S20, S22, S24, S27, S28, S30, S32, S33, S36, S37, S38, S40, S42, S44, S47, S49, S50, S52 + 1 additional
Good (4.0–4.49)	24	43.6%	S02, S03, S05, S06, S09, S14, S16, S18, S19, S21, S25, S26, S29, S31, S34, S35, S39, S43, S45, S6, S48, S51 + 2 additional
Moderate (<4.0)	3	5.5%	S12, S23, S41

Note: The full 55-row per-study quality table (detailed QA1–QA5 scores by study identifier S01–S55) is available from the corresponding author upon request and will be deposited as supplementary material upon acceptance.

2. METHOD

This review follows the systematic-review guidelines of Kitchenham and Brereton [18], organized in three phases (planning, conducting, reporting), and adheres to PRISMA 2020 reporting.

2.1. Search strategy

A Boolean query was applied to Scopus, Web of Science, Research4Life, and ScienceDirect: (“deep learning” OR “segmentation”) AND (“neovascular AMD” OR “nAMD” OR “wet AMD” OR “intraretinal fluid” OR “subretinal fluid”) AND (“OCT” OR “optical coherence tomography”). Searches were last

executed on 20 January 2026 (Scopus export date); the eligibility window was restricted to 2021–2025, so a small number of early-access records dated 2026 retrieved by the January 2026 query were excluded. Backward snowballing was applied to the reference lists of all eligible studies.

2.2. Study selection

The search retrieved 252 records, distributed by source as follows: Scopus (n = 123), ScienceDirect (n = 42), Web of Science (n = 35), and Research4Life (n = 52). After removal of 14 duplicates, 238 unique records were screened at full text. Applying the criteria in Table 3, 183 records were excluded—off-topic or non-nAMD studies including central serous chorioretinopathy (n ≈ 67), classification without fluid quantification (n ≈ 44), review articles (n ≈ 25), classical machine learning or image processing (n ≈ 17), and non-OCT modalities (n ≈ 10). Two studies (RetFluidNet [6] and the curvature-loss network [7]) are reported as backward-snowballing additions. The final corpus comprised 55 included studies published in 2021–2025: 53 identified through database searching and 2 through backward snowballing. Records carrying a 2026 early-access date were excluded to keep the review window closed at 2021–2025; eligible 2021–2025 studies were retained in their place so that the included count was unaffected. The complete identification, screening, and inclusion process is summarized in Figure 2.

Classical machine-learning and image-processing-only studies (EC3) were excluded because the review targets the representational and generalization behavior specific to end-to-end deep-learning segmentation, which classical pipelines do not exhibit.

Table 3. Inclusion and exclusion criteria

Inclusion (IC)	Exclusion (EC)
IC1 : nAMD/wet AMD studies	EC1 : Other retinal diseases (DR, glaucoma, dry AMD, CSCR)
IC2 : OCT/OCTA imaging, human subjects	EC2 : Non-OCT imaging (fundus, MRI)
IC3 : Deep-learning methods	EC3 : Classical ML / image processing only
IC4 : Fluid segmentation/quantification (IRF, SRF, PED, SHRM)	EC4 : Classification-only, no localization

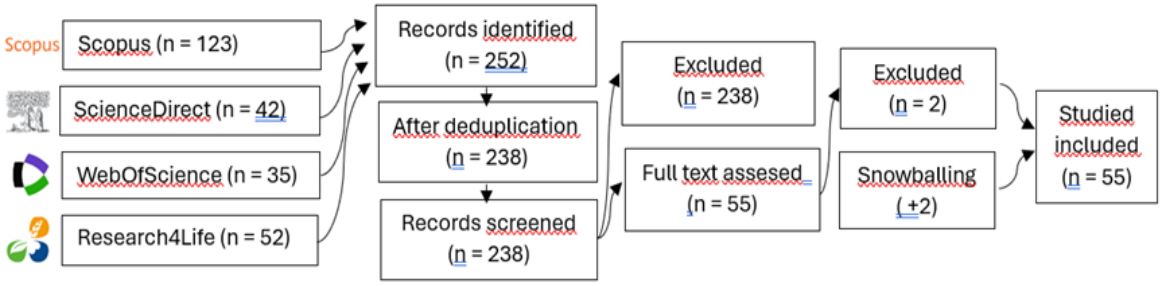

Figure 2. PRISMA 2020 flow diagram of study identification, screening, eligibility, and inclusion

2.3. Quality assessment

Each study was appraised on five criteria as shown in Table 4, scored 0–1 (half-points permitted; maximum 5). Studies scoring ≥ 4.5 were rated high-quality, 4.0–4.5 good-quality, and < 4.0 moderate-quality. Two reviewers scored every study independently: the first author and the supervising professor. In Figure 3, across the 55 included studies, the two raters assigned the same quality category in 52 cases (94.5% raw agreement); the three disagreements concerned dataset documentation (QA3) and were resolved by consensus as shown in Figure 3(a). Inter-rater agreement was almost perfect (Cohen's $\kappa = 0.89$) as shown in Figure 3(b). The corpus comprised 28 high-quality (50.9%), 24 good-quality (43.6%), and 3 moderate-quality (5.5%) studies. Mean per-criterion scores were QA1 = 0.97, QA2 = 0.95, QA3 = 0.83, QA4 = 0.96, and QA5 = 0.64 (SD = 0.23). The low QA5 mean reflects limited real-world validation in several studies and the documented difficulty of grading SHRM, whose heterogeneous appearance makes manual delineation less consistent than for the fluid compartments [15], [19]. Half-points were assigned when a criterion was partially met—for example, QA3 = 0.5 when dataset size was reported but the OCT vendor was not. Similar SLR methodology has been applied in adjacent AI-for-health domains [20], [21].

Table 4. Quality-assessment criteria

Criterion	Operational definition
QA1	Clarity of objectives and research questions
QA2	Methodological transparency sufficient for replication
QA3	Dataset documentation (size, source, OCT vendor)
QA4	Evaluation rigor (quantitative metrics, baseline comparison)
QA5	Clinical relevance (real-world validation or translational discussion)

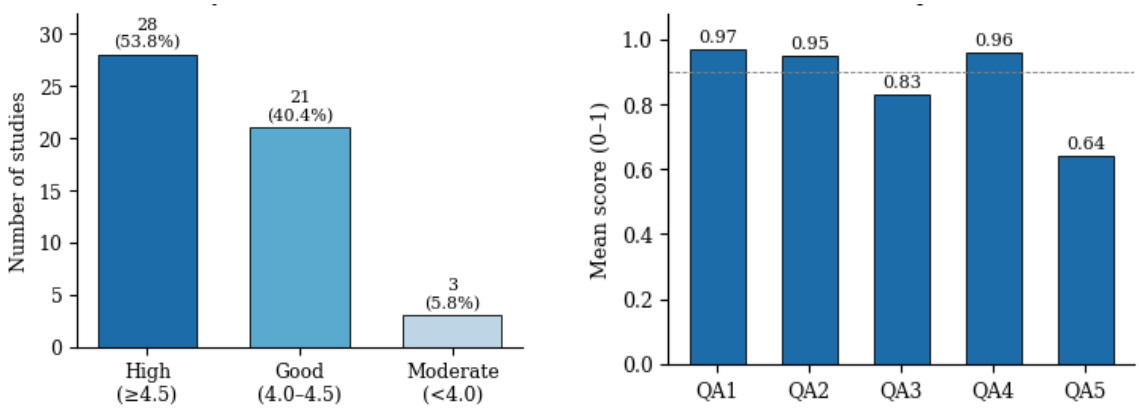

Figure 3. Quality-assessment outcomes (a) distribution of the 55 graded studies across quality levels: 28 high-quality (≥ 4.5), 24 good-quality (4.0–4.49), 3 moderate-quality (< 4.0) and (b) mean score per criterion (QA1–QA5). Inter-rater agreement Cohen's κ = 0.89

2.4. Data extraction

A structured protocol captured study metadata (authors, year, venue), architecture category, dataset provenance and scale, targeted fluid types (IRF, SRF, PED, SHRM), performance metrics (dice, IoU, MAE), domain-adaptation strategy, and level of clinical validation.

3. RESULTS AND DISCUSSION

3.1. Architectural evolution (RQ1)

Architectural development traced a clear trajectory from encoder–decoder CNNs toward hybrid frameworks and, recently, self-supervised pre-training. Early work extended U-Net with multi-scale context. Hassan *et al.* [5] integrated atrous spatial pyramid pooling into a CNN backbone for multi-class fluid segmentation across vendors. RetFluidNet augmented an encoder–decoder with enhanced skip connections and atrous convolutions [6]. A curvature-regularization term in the loss enforced shape priors and improved boundary continuity [7].

Attention and relational modeling followed. Liu *et al.* [8] embedded attention gating to focus capacity on diagnostically relevant regions, improving IRF sensitivity. Graph-based methods then introduced topological reasoning: a graph-attention U-Net encoded inter-layer relationships [9], and a GCN-assisted attention-guided U-Net reduced false positives in low-contrast regions [10]. Loss-balanced parallel decoding separated region and boundary optimization [22], while multi-scale fusion attention-residual designs (MCFAR-net) and edge-attention autoencoders refined fluid contours [23], [24].

To capture long-range context, GLTNet combined convolutional encoders with multi-scale Transformer modules [12], and FNeXter proposed a ConvNeXt–Transformer hybrid with self-adaptive fusion [11]. RetiFluidNet combined dual-attention with multi-scale deep supervision [25], and DAA-UNet merged dense connectivity, atrous pooling, and attention gating [26]. A cross-Transformer with uncertainty guidance and a cascaded attention-fusion U-Net targeted low-quality scans [27], [28], while a lightweight fully convolutional network prioritized efficiency [29]. Complementary designs address specific compartments and modalities: a fuzzy-rough-set feature-discretization CNN (FRCNN) targeted noise-robust SRF segmentation [30], and a Y-shaped spiking neural network explored energy-efficient retinal-layer segmentation [31]. On OCT angiography (OCTA), a multilateral interaction-enhanced graph convolutional network (MTG-Net) jointly segmented CNV regions and vessels and released the public CNVSeg dataset [32], while MTD-Net

applied multi-task discriminative learning for robust CNV delineation [33]. Figure 4 traces this architectural progression. Table 5 summarizes representative architectures and Table 6 contrasts strategy families.

A self-supervised paradigm has emerged. Time-equivariant non-contrastive pre-training (3DTINC) [34] and longitudinal morphing self-supervision (Morph-SSL) [35] improve disease-progression prediction. A related subset of the corpus moves beyond segmentation toward prediction and generation: LamNet predicted CNV volume from SD-OCT using lesion-attention maps [36], a hybrid model forecast three-dimensional CNV growth from longitudinal OCT [37], and generative approaches synthesized post-therapeutic OCT appearance through single-horizon disease-evolution learning [38], a biomarkers-aware bibranch GAN [39], and a spatiotemporal evolution-aware adversarial diffusion framework [40]. These are pre-training and prediction frameworks rather than dedicated segmentation models; their relevance is as a route to label efficiency and domain generalization, not as segmentation benchmarks.

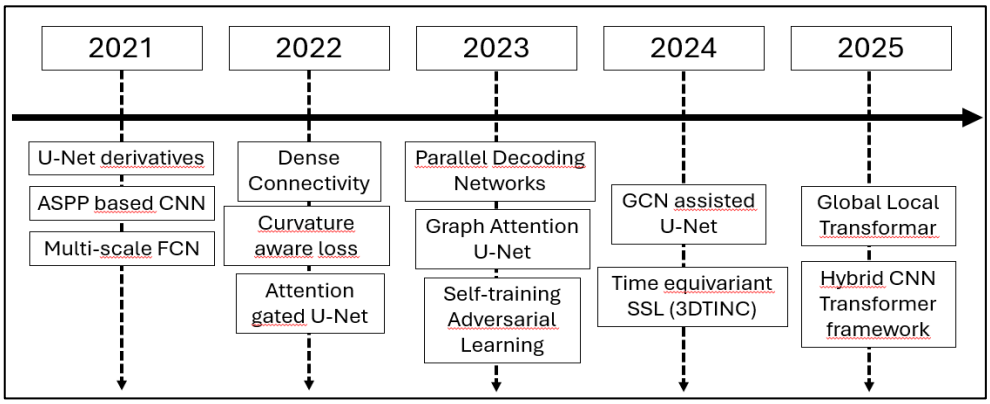

Figure 4. Evolution of deep-learning architectures for nAMD OCT fluid segmentation, from CNN-based U-Net derivatives toward hybrid global–local and self-supervised foundation models (2021–2025)

Table 5. Representative architectures

Model	Backbone	Key innovation	Ref
RFS-Net	CNN	ASPP + residual/inception encoder	[5]
RetFluidNet	U-Net	Enhanced skip + atrous convolutions	[6]
Curvature-loss network	FCN	Curvature regularization for boundaries	[7]
Attention U-Net	U-Net	Attention gating for IRF sensitivity	[8]
Graph Attention U-Net	U-Net + GCN	Topological relational reasoning	[9]
GCN-assisted U-Net	CNN + GCN	Graph convolution + attention fusion	[10]
FNeXter	ConvNeXt + Transformer	Self-adaptive multi-scale fusion	[11]
GLTNet	CNN + Transformer	Global–local long-range context	[12]
RetiFluidNet	CNN + Attention	Dual-attention + deep supervision	[25]
DAA-UNet	Dense U-Net	Dense + ASPP + attention	[26]
FRCNN	CNN + fuzzy-rough sets	Feature discretization for SRF under noise	[30]
Y-shaped SNN	Spiking neural network	Energy-efficient layer segmentation	[31]
MTG-Net (OCTA)	Multi-task + GCN	Region–vessel graph reasoning; CNVSeg	[32]
MTD-Net (OCTA)	Multi-task CNN	Discriminative CNV delineation	[33]
3DTINC / Morph-SSL	SSL Transformer	Self-supervised progression modeling	[34],[35]
LamNet	CNN + attention maps	CNV volume prediction	[36]
Generative predictors	GAN / diffusion	Post-therapeutic OCT synthesis	[38]–[40]

Table 6. Strategy families: strengths and limitations

Strategy	Strengths	Limitations
CNN	Local precision; efficient	Limited global context; weak transfer
Attention-CNN	Feature selectivity; fewer false positives	Constrained attention range
Graph-based	Relational/topological reasoning	High complexity; limited scalability
Transformer	Long-range global context	Memory cost; data-hungry
Hybrid CNN–Transformer	Local + global balance	Architectural/tuning complexity
Foundation model (SSL)	Annotation-efficient; generalizable	Costly pre-training; nascent for segmentation

3.2. Datasets, annotation, and domain generalization (RQ2)

Public corpora such as RETOUCH underpin reproducible benchmarking; it provides multi-vendor data (Cirrus, Spectralis, Topcon) from two clinical centers with all three fluid types annotated [41]. Figure 5 maps the principal datasets and illustrates cross-vendor performance variability. AMD-SD adds 3,049 B-scans from 138 patients with five labels including SHRM [19], and AROI offers 1,136 B-scans from 24 patients with layer and IRF/SRF/PED annotations [42]. OCTA-based corpora are emerging alongside structural OCT, including the public CNVSeg dataset [32] and clinical OCTA cohorts used to train CNV segmentation [43], with semantic-guided latent-diffusion augmentation proposed to enlarge scarce OCTA training sets [44]. Models trained only on curated benchmarks may overstate real-world performance; clinical-cohort validation remains comparatively scarce [3]. Table 7 summarizes the principal datasets, with vendor and scale populated from the original sources.

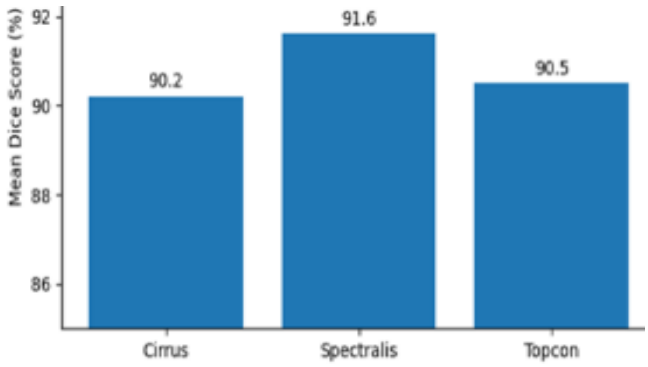

Figure 5. Cross-vendor segmentation performance variability across OCT platforms (Cirrus, Spectralis, Topcon), illustrating the domain-shift challenge

Device-level differences in resolution, intensity scaling, and speckle degrade cross-vendor performance. Several strategies address this: self-training adversarial adaptation with image- and feature-level alignment [13]; random-style augmentation for generalized segmentation [45]; and boundary-repairing dual-path modeling under PED [46]. Point-annotation enhancement with superpixel and confident-learning guidance reduces labeling burden in semi-supervised fluid segmentation [47]. Benchmark analyses confirm that cross-vendor generalization remains incompletely solved [41]. Manual labeling is subjective; SHRM is particularly ambiguous because of its heterogeneous composition [14], [15], establishing a ground-truth ceiling that automated systems rarely exceed.

Table 7. Principal OCT datasets (vendor and scale populated from source publications)

Dataset	Type	OCT vendor/scale	Ref
RETOUCH	Public	Multi-vendor (Cirrus, Spectralis, Topcon); 2 centers; all 3 fluids	[41]
AMD-SD	Public	Vendor not reported; 3,049 B-scans/138 patients; 5 labels incl. SHRM	[19]
AROI	Public	Vendor not reported; 1,136 B-scans/24 patients; layers + IRF/SRF/PED	[42]
Lausanne cohort	Private	Spectralis; 107 volumes; repeatability reported	[3]

3.3. Comparative segmentation performance (RQ3)

Across the corpus, IRF is consistently the most difficult compartment (Dice ≈ 0.762 [5]; ≈ 0.800 [6]), constrained by small lesion size, low contrast, speckle, and class imbalance [6], [7]. SRF and PED reach substantially higher accuracy (RetFluidNet: SRF 0.955, PED 0.927 [6]). The relative ordering of SRF and PED is not uniform across confirmed studies—RFS-Net reports PED 0.805 > SRF 0.796 [5], whereas RetFluidNet reports SRF > PED [6]—so only the position of IRF as the hardest compartment is consistent. This nuance is more defensible than asserting a fixed SRF > PED > IRF ordering. Figure 6 contrasts the confirmed per-compartment Dice values across reference models. Table 8 reports the per-compartment Dice values that bibliographic validation confirmed against the source papers. Daanouni *et al.* [48] reported comparable per-compartment performance (IRF 0.787, SRF 0.927, PED 0.897).

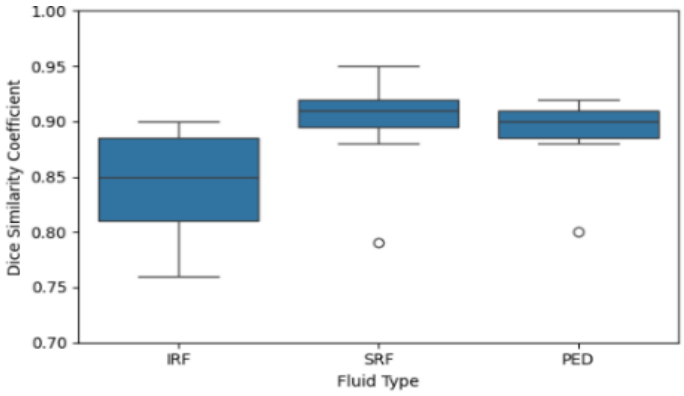

Figure 6. Per-compartment dice coefficients across confirmed reference models. IRF is consistently the hardest compartment; the relative ordering of SRF and PED is not uniform across studies

Table 8. Confirmed per-compartment dice

Model	IRF	SRF	PED	Ref
RFS-Net	0.762	0.796	0.805	[5]
RetFluidNet	0.800	0.955	0.927	[6]
Daanouni *et al.* [48]	0.787	0.927	0.897	[48]

Caution: values originate from different datasets, protocols, and ground-truth standards; they do NOT constitute a head-to-head benchmark and must not be read as a direct comparison.

The difficulty of IRF is governed primarily by intrinsic imaging properties lesion dimensions near the resolution limit, low contrast, speckle, and severe class imbalance rather than by architecture alone [6], [7]. Curvature-aware regularization partially mitigates boundary discontinuities but does not remove the small-lesion, low-contrast obstacle [7]. Crucially, overlap accuracy and clinical value can diverge: Mantel *et al.* [3] reported fluid-volume correlation coefficients approaching 0.99 for IRF and SRF despite imperfect pixel-level segmentation (dice 0.73 IRF, 0.67 SRF, 0.82 PED). Evaluation should therefore weight reproducible, clinically actionable volume estimation alongside dice.

SHRM is a heterogeneous subretinal finding (fibrin, neovascular tissue, blood, fibrosis) associated with worse visual outcomes [14]. Whole-volume systems that segment SHRM alongside IRF/SRF/PED report lower, more variable Dice for SHRM [15], and SHRM presence reduces pointwise retinal sensitivity by 5.13 dB—a larger functional impact than IRF or SRF in isolation [14]. The three-compartment framework is therefore no longer sufficient; future benchmarks should report SHRM explicitly.

3.4. Clinical translation (RQ4)

Deep learning has shifted nAMD assessment from qualitative inspection toward quantitative biomarker extraction. Mantel *et al.* [3] demonstrated high-repeatability volumetric quantification concordant with expert annotation, and automated quantification of macular fluid tracked response to anti-VEGF therapy [49]. Predictive modeling from OCT-derived fluid features can stratify treatment requirements and treat-and-extend intervals [50]. Real-world cohorts show that automated fluid monitoring supports interval extension while preserving vision [51], [52], captures recurrence patterns missed by qualitative grading [53], and quantifies biomarker change under newer agents such as faricimab and high-dose aflibercept [54]–[56]. Multimodal links between residual fluid and OCT-angiography parameters [57], OCTA-derived deep-learning markers of anti-VEGF response [58], and associations between fluid and aqueous cytokines [59] further extend the clinical picture. Beyond fluid itself, automated photoreceptor-integrity quantification predicted persistent disease activity [60], patient-operated home OCT with automated fluid detection enabled daily self-monitoring [61], fully automatic three-dimensional fluid visualization supported clinical interpretation of OCT cubes [62], and an intelligent decision-support system targeted early diagnosis of macular pathology [63].

A distinction separates research prototypes from clinically validated tools: most reviewed architectures remain research-stage [9], [11], whereas deployment requires demonstrated robustness across devices, sites, and populations. The primary determinant of clinical adoptability is sustained volumetric consistency over time and across vendors, rather than peak benchmark accuracy [3]. Incorporating SHRM into regulatory-grade tools is a logical next step given its functional impact [14].

3.5. Research gaps and future directions

Five gaps emerge, each mapped to a concrete future direction as shown in Table 9. Notably, imaging artifacts (shadowing, attenuation) are explicitly paired with a dedicated direction on artifact-robust preprocessing and standardization, addressing the previous disconnect between identified gaps and proposed directions.

Table 9. Gap-to-future-direction mapping

Identified gap	Mapped future direction
IRF small-lesion / low-contrast difficulty	IRF-specialized architectures and task-specific for small, low-contrast lesions
Imaging artifacts (shadowing, attenuation)	Artifact-robust preprocessing and standardized image-quality normalization protocols
Cross-vendor domain shift	Multi-vendor training, domain adaptation, federated and self-supervised learning
Dice-based evaluation limits	Standardized volumetric-reliability and longitudinal-consistency metrics beyond Dice
SHRM under-segmentation	Four-biomarker benchmarks that report SHRM performance explicitly
Annotation scarcity / variability	Semi-supervised and foundation-model pipelines with consensus annotation

This review has limitations. The 2021–2025 scope may omit earlier foundational work. Publication bias likely skews the corpus toward high-performing models. Reporting heterogeneity precludes direct cross-study comparison; the confirmed per-compartment Dice values derive from different datasets and ground-truth standards and are not directly comparable. The exclusive focus on nAMD excludes transferable methods from adjacent retinal diseases.

4. CONCLUSION

This systematic review synthesized 55 studies (2021–2025) on deep-learning fluid segmentation in nAMD OCT. Architectures progressed from CNNs toward attention-based, graph-based, and hybrid CNN–Transformer designs, with self-supervised pre-training emerging as a route to label efficiency and domain generalization. IRF remains the most difficult classic compartment, and SHRM is establishing itself as a clinically important fourth biomarker that current pipelines rarely target. Generalizability is bounded by dataset heterogeneity and cross-vendor domain shift, and the dice coefficient is an incomplete proxy for clinical value, since volumetric reproducibility better predicts clinical utility. Translating high-performing research models into deployable decision-support tools will require SHRM-aware architectures, standardized multi-compartment and volumetric evaluation, artifact-robust preprocessing, robust domain adaptation, and large-scale prospective validation.

FUNDING INFORMATION

The authors state no funding was involved.

AUTHOR CONTRIBUTIONS STATEMENT

This journal uses the Contributor Roles Taxonomy (CRediT) to recognize individual author contributions, reduce authorship disputes, and facilitate collaboration.

Name of Author	C	M	So	Va	Fo	I	R	D	O	E	Vi	Su	P	Fu
Driss Rifai	✓	✓		✓	✓	✓	✓	✓	✓	✓	✓		✓	
Ahmed Zellou	✓	✓		✓	✓					✓		✓		

C : **C**onceptualization
M : **M**ethodology
So : **So**ftware
Va : **Va**lidation
Fo : **Fo**rmal analysis
I : **I**nvestigation
R : **R**esources
D : **D**ata Curation
O : Writing - **O**riginal Draft
E : Writing - Review & **E**diting
Vi : **Vi**sualization
Su : **Su**pervision
P : **P**roject administration
Fu : **Fu**nding acquisition

CONFLICT OF INTEREST STATEMENT

The authors declare no conflict of interest.

DATA AVAILABILITY

The data supporting this study's findings are available from the corresponding author upon reasonable request.

REFERENCES

[1] W. L. Wong *et al.*, "Global prevalence of age-related macular degeneration and disease burden projection for 2020 and 2040: a systematic review and meta-analysis," *The Lancet Global Health*, vol. 2, no. 2, pp. e106–e116, Feb. 2014, doi: 10.1016/s2214-109x(13)70145-1.

[2] U. Schmidt-Erfurth *et al.*, "AI-based monitoring of retinal fluid in disease activity and under therapy," *Progress in Retinal and Eye Research*, vol. 86, p. 100972, Jan. 2022, doi: 10.1016/j.preteyeres.2021.100972.

[3] I. Mantel *et al.*, "Automated quantification of pathological fluids in neovascular age-related macular degeneration, and its repeatability using deep learning," *Translational Vision Science & Technology*, vol. 10, no. 4, p. 17, Apr. 2021, doi: 10.1167/tvst.10.4.17.

[4] S. Dong, P. Wang, and K. Abbas, "A survey on deep learning and its applications," *Computer Science Review*, vol. 40, p. 100379, May 2021, doi: 10.1016/j.cosrev.2021.100379.

[5] B. Hassan *et al.*, "Deep learning based joint segmentation and characterization of multi-class retinal fluid lesions on OCT scans for clinical use in anti-VEGF therapy," *Computers in Biology and Medicine*, vol. 136, p. 104727, 2021, doi: 10.1016/j.compbiomed.2021.104727.

[6] L. B. Sappa *et al.*, "RetFluidNet: retinal fluid segmentation for SD-OCT images using convolutional neural network," *Journal of Digital Imaging*, vol. 34, no. 3, pp. 691–704, 2021, doi: 10.1007/s10278-021-00459-w.

[7] G. Xing *et al.*, "Multi-scale pathological fluid segmentation in OCT with a novel curvature loss in convolutional neural network," *IEEE Transactions on Medical Imaging*, vol. 41, no. 6, pp. 1547–1559, 2022, doi: 10.1109/tmi.2022.3142048.

[8] X. Liu, S. Wang, Y. Zhang, D. Liu, and W. Hu, "Automatic fluid segmentation in retinal optical coherence tomography images using attention based deep learning," *Neurocomputing*, vol. 452, pp. 576–591, 2021, doi: 10.1016/j.neucom.2020.07.143.

[9] Y. Shen *et al.*, "Graph attention U-Net for retinal layer surface detection and choroid neovascularization segmentation in OCT images," *IEEE Transactions on Medical Imaging*, vol. 42, no. 11, pp. 3140–3154, Nov. 2023, doi: 10.1109/tmi.2023.3240757.

[10] D. Oh *et al.*, "GCN-assisted attention-guided UNet for automated retinal OCT segmentation," *Expert Systems with Applications*, vol. 249, p. 123620, 2024, doi: 10.1016/j.eswa.2024.123620.

[11] Z. Niu *et al.*, "FNeXter: a multi-scale feature fusion network based on ConvNeXt and transformer for retinal OCT fluid segmentation," *Sensors*, vol. 24, no. 8, p. 2425, Apr. 2024, doi: 10.3390/s24082425.

[12] F. Li, H. Wei, X. Sheng, Y. Chen, H. Zou, and S. Huang, "Global-local transformer network for automatic retinal pathological fluid segmentation in optical coherence tomography images," *Computer Methods and Programs in Biomedicine*, vol. 266, p. 108772, 2025, doi: 10.1016/j.cmpb.2025.108772.

[13] X. Li, S. Niu, X. Gao, X. Zhou, J. Dong, and H. Zhao, "Self-training adversarial learning for cross-domain retinal OCT fluid segmentation," *Computers in Biology and Medicine*, vol. 155, p. 106650, Mar. 2023, doi: 10.1016/j.compbiomed.2023.106650.

[14] G. S. Reiter *et al.*, "Deep-learning–based analysis of disease-specific structural biomarkers on retinal sensitivity in neovascular age-related macular degeneration," *Investigative Ophthalmology & Visual Science*, vol. 66, no. 12, p. 68, 2025, doi: 10.1167/iovs.66.12.68.

[15] F. Ricardi *et al.*, "Validation of a deep learning model for automatic detection and quantification of five OCT critical retinal features associated with neovascular age-related macular degeneration," *British Journal of Ophthalmology*, vol. 108, no. 10, pp. 1436–1442, Mar. 2024, doi: 10.1136/bjo-2023-324647.

[16] D. S. Ting *et al.*, "Deep learning in ophthalmology: the technical and clinical considerations," *Progress in retinal and eye research*, vol. 72, p. 100759, 2019.

[17] M. Lin, G. Bao, X. Sang, and Y. Wu, "Recent advanced deep learning architectures for retinal fluid segmentation on optical coherence tomography images," *Sensors*, vol. 22, no. 8, p. 3055, Apr. 2022, doi: 10.3390/s22083055.

[18] B. Kitchenham and P. Brereton, "A systematic review of systematic review process research in software engineering," *Information and Software Technology*, vol. 55, no. 12, pp. 2049–2075, Dec. 2013, doi: 10.1016/j.infsof.2013.07.010.

[19] Y. Hu *et al.*, "AMD-SD: an optical coherence tomography image dataset for wet AMD lesions segmentation," *Scientific Data*, vol. 11, no. 1, 2024, doi: 10.1038/s41597-024-03844-6.

[20] A. Berquedich and A. Zellou, "A quality assessment study of deep learning techniques for medical image diagnosis and their applications: a systematic literature review," *International Journal of Advanced Computer Science and Applications*, vol. 16, no. 10, 2025, doi: 10.14569/ijacsa.2025.0161032.

[21] L. Ajallouda, F. Z. Fagroud, A. Zellou, and E. habib Benlahmar, "A systematic literature review of keyphrases extraction approaches," *International Journal of Interactive Mobile Technologies (iJIM)*, vol. 16, no. 16, pp. 31–58, Aug. 2022, doi: 10.3991/ijim.v16i16.33081.

[22] X. Yu *et al.*, "Loss-balanced parallel decoding network for retinal fluid segmentation in OCT," *Computers in Biology and Medicine*, vol. 165, p. 107319, Oct. 2023, doi: 10.1016/j.compbiomed.2023.107319.

[23] P. Geetha Pavani *et al.*, "A robust segmentation of retinal fluids from OCT images using MCFAR-net," *Neurocomputing*, vol. 599, p. 128059, 2024, doi: 10.1016/j.neucom.2024.128059.

[24] G. P. Pappu, S. Tankala, K. Talabhaktula, and B. Biswal, "<scp>EANet</scp>: Multiscale autoencoder based edge attention network for fluid segmentation from <scp>SD-OCT</scp> images," *International Journal of Imaging Systems and Technology*, vol. 33, no. 3, pp. 909–927, Dec. 2022, doi: 10.1002/ima.22840.

[25] R. Rasti, A. Biglari, M. Rezapourian, Z. Yang, and S. Farsiu, "RetiFluidNet: A self-adaptive and multi-attention deep convolutional network for retinal OCT fluid segmentation," *IEEE Transactions on Medical Imaging*, vol. 42, no. 5, pp. 1413–1423, May 2023, doi: 10.1109/tmi.2022.3228285.

[26] T. Hu, J. Ding, Y. Liu, Y. Zhang, and L. Yang, "DAA-UNet: a dense connectivity and atrous spatial pyramid pooling attention UNet model for retinal optical coherence tomography fluid segmentation," *IET Software*, vol. 2025, no. 1, Jan. 2025, doi: 10.1049/sfw2/6006074.

[27] H. Liu *et al.*, "Semantic uncertainty guided cross-transformer for enhanced macular edema segmentation in OCT images," *Computers in Biology and Medicine*, vol. 174, p. 108458, May 2024, doi: 10.1016/j.compbiomed.2024.108458.

[28] Z. Wu *et al.*, "Harmonizing Unets: attention fusion module in cascaded-Unets for low-quality OCT image fluid segmentation," *Computers in Biology and Medicine*, vol. 183, p. 109223, Dec. 2024, doi: 10.1016/j.compbiomed.2024.109223.

[29] E. Parra-Mora and L. A. da Silva Cruz, "LOCTseg: A lightweight fully convolutional network for end-to-end optical coherence tomography segmentation," *Computers in Biology and Medicine*, vol. 150, p. 106174, Nov. 2022, doi: 10.1016/j.compbiomed.2022.106174.
[30] Q. Chen, L. Zeng, and W. Ding, "FRCNN: A combination of fuzzy-rough-set-based feature discretization and convolutional neural network for segmenting subretinal fluid lesions," *IEEE Transactions on Fuzzy Systems*, vol. 33, no. 1, pp. 350–364, Jan. 2025, doi: 10.1109/tfuzz.2024.3473310.
[31] B. Yang, Y. Huang, Y. Xie, J. Li, and Q. Hao, "A Y-shaped spiking neural network for automatic retinal segmentation," *Optics and Lasers in Engineering*, vol. 198, p. 109512, Mar. 2026, doi: 10.1016/j.optlaseng.2025.109512.
[32] T. Chen *et al.*, "Neovascularization segmentation via a multilateral interaction-enhanced graph convolutional network," *IEEE Transactions on Pattern Analysis and Machine Intelligence*, vol. 47, no. 12, pp. 11107–11123, Dec. 2025, doi: 10.1109/tpami.2025.3600335.
[33] D. Zhang *et al.*, "MTD-Net: A robust multi-task discriminative network for choroidal neovascularization segmentation," *Pattern Recognition*, vol. 172, p. 112697, Apr. 2026, doi: 10.1016/j.patcog.2025.112697.
[34] T. Emre *et al.*, "3DTINC: time-equivariant non-contrastive learning for predicting disease progression from longitudinal OCTs," *IEEE Transactions on Medical Imaging*, vol. 43, no. 9, pp. 3200–3210, 2024, doi: 10.1109/tmi.2024.3391215.
[35] A. Chakravarty *et al.*, "Morph-SSL: self-supervision with longitudinal morphing for forecasting AMD progression from OCT volumes," *IEEE Transactions on Medical Imaging*, vol. 43, no. 9, pp. 3224–3239, 2024, doi: 10.1109/tmi.2024.3390940.
[36] Y. Zhang, X. Ma, M. Li, Z. Ji, S. Yuan, and Q. Chen, "LamNet: A lesion attention maps-guided network for the prediction of choroidal neovascularization volume in SD-OCT images," *IEEE Journal of Biomedical and Health Informatics*, vol. 26, no. 4, pp. 1660–1671, Apr. 2022, doi: 10.1109/jbhi.2021.3129462.
[37] Q. Meng *et al.*, "Three-dimensional choroid neovascularization growth prediction from longitudinal retinal OCT images based on a hybrid model," *Pattern Recognition Letters*, vol. 146, pp. 108–114, 2021, doi: 10.1016/j.patrec.2021.03.006.
[38] Y. Zhang, K. Huang, M. Li, S. Yuan, and Q. Chen, "Learn single-horizon disease evolution for predictive generation of post-therapeutic neovascular age-related macular degeneration," *Computer Methods and Programs in Biomedicine*, vol. 230, p. 107364, Mar. 2023, doi: 10.1016/j.cmpb.2023.107364.
[39] P. Zhao *et al.*, "Biomarkers-aware asymmetric bibranch GAN with adaptive memory batch normalization for prediction of anti-VEGF treatment response in neovascular age-related macular degeneration," *IEEE Journal of Biomedical and Health Informatics*, vol. 28, no. 1, pp. 557–568, Jan. 2024, doi: 10.1109/jbhi.2023.3302989.
[40] X. Li, Y. Zhang, S. Niu, S. Yuan, and Q. Chen, "From discrete to continuous: A spatiotemporal evolution-aware adversarial diffusion framework for retinal disease progression prediction," *Neurocomputing*, vol. 660, p. 131873, Jan. 2026, doi: 10.1016/j.neucom.2025.131873.
[41] H. Bogunovic *et al.*, "RETOUCH: The retinal OCT fluid detection and segmentation benchmark and challenge," *IEEE Transactions on Medical Imaging*, vol. 38, no. 8, pp. 1858–1874, Aug. 2019, doi: 10.1109/tmi.2019.2901398.
[42] M. Melinščak, M. Radmilović, Z. Vatavuk, and S. Lončarić, "Annotated retinal optical coherence tomography images (AROI) database for joint retinal layer and fluid segmentation," *Automatika*, vol. 62, no. 3–4, pp. 375–385, Aug. 2021, doi: 10.1080/00051144.2021.1973298.
[43] W. Feng *et al.*, "Automated segmentation of choroidal neovascularization on optical coherence tomography angiography images of neovascular age-related macular degeneration patients based on deep learning," *Journal of Big Data*, vol. 10, no. 1, 2023, doi: 10.1186/s40537-023-00757-w.
[44] D. I. Morís, J. de Moura, E. J. Carmona, J. Novo, and M. Ortega, "Semantic-guided generative latent diffusion augmentation approaches for improving the neovascularization diagnosis in OCT-A imaging," *Pattern Recognition Letters*, vol. 189, pp. 31–37, Mar. 2025, doi: 10.1016/j.patrec.2025.01.003.
[45] C. Lu *et al.*, "RSAPower: random style augmentation driven structure perception network for generalized retinal OCT fluid segmentation," *IEEE Transactions on Medical Imaging*, vol. 44, no. 5, pp. 2353–2367, May 2025, doi: 10.1109/tmi.2025.3531496.
[46] X. Liu, X. Li, Y. Zhang, M. Wang, J. Yao, and J. Tang, "Boundary-repairing dual-path network for retinal layer segmentation in OCT image with pigment epithelial detachment," *Journal of Imaging Informatics in Medicine*, vol. 37, no. 6, pp. 3101–3130, May 2024, doi: 10.1007/s10278-024-01093-y.
[47] T. Weng *et al.*, "Enhancing point annotations with superpixel and confident learning guided for improving semi-supervised OCT fluid segmentation," *Biomedical Signal Processing and Control*, vol. 94, p. 106283, Aug. 2024, doi: 10.1016/j.bspc.2024.106283.
[48] O. Daanouni, B. Cherradi, and A. Tmiri, "Automated end-to-end architecture for retinal layers and fluids segmentation on OCT B-scans," *Multimedia Tools and Applications*, vol. 84, no. 15, pp. 14305–14328, 2024, doi: 10.1007/s11042-024-19514-z.
[49] M. Michl *et al.*, "Automated quantification of macular fluid in retinal diseases and their response to anti-VEGF therapy," *British Journal of Ophthalmology*, vol. 106, no. 1, pp. 113–120, Oct. 2020, doi: 10.1136/bjophthalmol-2020-317416.
[50] H. Bogunović, V. Mares, G. S. Reiter, and U. Schmidt-Erfurth, "Predicting treat-and-extend outcomes and treatment intervals in neovascular age-related macular degeneration from retinal optical coherence tomography using artificial intelligence," *Frontiers in Medicine*, vol. 9, Aug. 2022, doi: 10.3389/fmed.2022.958469.
[51] V. Mares *et al.*, "Automated fluid monitoring to optimize the follow-up of neovascular age-related macular degeneration patients in the Brazilian population," *International Journal of Retina and Vitreous*, vol. 11, no. 1, 2025, doi: 10.1186/s40942-025-00695-0.
[52] V. Mares *et al.*, "Approved AI-based fluid monitoring to identify morphological and functional treatment outcomes in neovascular age-related macular degeneration in real-world routine," *British Journal of Ophthalmology*, vol. 108, no. 7, pp. 971–977, 2023, doi: 10.1136/bjo-2022-323014.
[53] V. Prenner *et al.*, "Dynamics and patterns of recurrence in neovascular AMD during real-world management using automated fluid monitoring," *Heliyon*, vol. 10, no. 10, p. e31567, May 2024, doi: 10.1016/j.heliyon.2024.e31567.
[54] M. Hafner *et al.*, "Deep learning assisted analysis of biomarker changes in refractory neovascular AMD after switch to faricimab," *International Journal of Retina and Vitreous*, vol. 11, no. 1, Apr. 2025, doi: 10.1186/s40942-025-00669-2.
[55] M. Hafner *et al.*, "Deep learning-assisted analysis of biomarker changes after increase of dosing from aflibercept 2 mg to 8 mg in therapy-resistant neovascular age-related macular degeneration," *BMJ Open Ophthalmology*, vol. 10, no. 1, p. e002176, May 2025, doi: 10.1136/bmjophth-2025-002176.
[56] M. Hafner *et al.*, "Deep-learning-assisted analysis of early biomarker changes in treatment-naïve patients with neovascular AMD under intravitreal faricimab," *Ophthalmology and Therapy*, vol. 14, no. 5, pp. 1025–1037, Mar. 2025, doi: 10.1007/s40123-025-01125-y.

[57] M. Schranz, H. Bogunovic, G. Deak, A. Sadeghipour, G. S. Reiter, and U. Schmidt-Erfurth, "Linking disease activity with optical coherence tomography angiography in neovascular age related macular degeneration using artificial intelligence," *Scientific Reports*, vol. 14, no. 1, Aug. 2024, doi: 10.1038/s41598-024-70234-8.
[58] S. Liu *et al.*, "Efficacy and prognostic factors of anti-VEGF treatment for neovascular age-related macular degeneration: An OCTA imaging-based deep learning analysis," *Photodiagnosis and Photodynamic Therapy*, vol. 55, p. 104701, Oct. 2025, doi: 10.1016/j.pdpdt.2025.104701.
[59] S. Song *et al.*, "Retinal fluid is associated with cytokines of aqueous humor in age-related macular degeneration using automatic 3-dimensional quantification," *Frontiers in Cell and Developmental Biology*, vol. 11, Mar. 2023, doi: 10.3389/fcell.2023.1157497.
[60] X. Song *et al.*, "Automatic quantification of retinal photoreceptor integrity to predict persistent disease activity in neovascular age-related macular degeneration using deep learning," *Frontiers in Neuroscience*, vol. 16, Aug. 2022, doi: 10.3389/fnins.2022.952735.
[61] T. D. L. Keenan, M. Goldstein, D. Goldenberg, D. Zur, S. Shulman, and A. Loewenstein, "Prospective, longitudinal pilot study," *Ophthalmology Science*, vol. 1, no. 2, p. 100034, 2021, doi: 10.1016/j.xops.2021.100034.
[62] E. López-Varela, P. L. Vidal, N. O. Pascual, J. Novo, and M. Ortega, "Fully-automatic 3D intuitive visualization of age-related macular degeneration fluid accumulations in OCT cubes," *Journal of Digital Imaging*, vol. 35, no. 5, pp. 1271–1282, May 2022, doi: 10.1007/s10278-022-00643-6.
[63] T. G. Kamenskikh, O. N. Dolinina, I. O. Kolbenev, and E. V Veselova, "An intelligent decision-making system for early diagnosis of macular pathology," *Russian Ophthalmological Journal*, vol. 15, no. 2 (Прил), pp. 69–74, 2022, doi: 10.21516/2072-0076-2022-15-2-supplement-69-74.

BIOGRAPHIES OF AUTHORS



Driss Rifai is a Ph.D. candidate at ENSIAS, Mohammed V University in Rabat, Morocco, affiliated with the Software Project Management (SPM) research team. His research focuses on deep learning for medical image analysis and AI applications in ophthalmology, with emphasis on OCT-based retinal fluid segmentation. He can be contacted at email: driss_rifai@um5.ac.ma.



Ahmed Zellou is a professor and head of the Software Project Management (SPM) research team at ENSIAS, Mohammed V University in Rabat, Morocco. He holds a PhD in Computer Science and has authored numerous publications in software engineering, AI, and healthcare informatics. He can be contacted at email: ahmed.zellou@um5.ac.ma.